arXiv:0811.4396v4 [cond-mat.mtrl-sci] 15 Jul 2009

A tight-binding approach to uniaxial strain in graphene

Vitor M. Pereira and A. H. Castro Neto
Department of Physics, Boston University, 590 Commonwealth Avenue, Boston, MA 02215, USA

N. M. R. Peres
Centro de Física e Departamento de Física, Universidade do Minho, P-4710-057, Braga, Portugal

(Dated: February 12, 2022)

We analyze the effect of tensional strain in the electronic structure of graphene. In the absence of electron-electron interactions, within linear elasticity theory, and a tight-binding approach, we observe that strain can generate a bulk spectral gap. However this gap is critical, requiring threshold deformations in excess of 20%, and only along preferred directions with respect to the underlying lattice. The gapless Dirac spectrum is robust for small and moderate deformations, and the gap appears as a consequence of the merging of the two inequivalent Dirac points, only under considerable deformations of the lattice. We discuss how strain-induced anisotropy and local deformations can be used as a means to affect transport characteristics and pinch off current flow in graphene devices.

PACS numbers: 81.05.Uw,62.20.-x,73.90.+f
Keywords: graphene, strain, elasticity, electronic structure, tight-binding

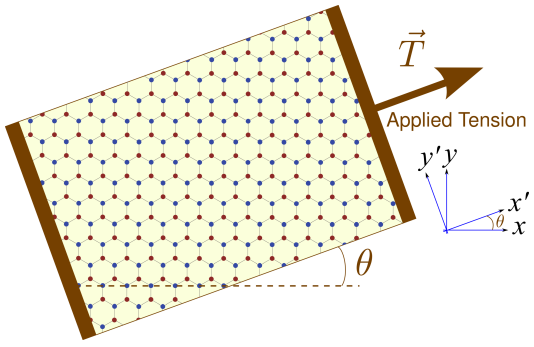
It is now well established that sp^2 bonded carbon systems feature record-breaking mechanical strength and stiffness. Investigations in the context of carbon nanotubes reveal intrinsic strengths[1] that make these systems the strongest in nature, Recently, graphene — the mother of all sp^2 carbon structures — has been confirmed as the strongest material ever to be measured[2], being able to sustain reversible elastic deformations in excess of 20%[3].

These mechanical measurements arise at a time where graphene draws considerable attention on account of its unusual and rich electronic properties. Besides the great crystalline quality, high mobility and resilience to high current densities[4], they include a strong field effect[5], absence of backscattering[6] and a minimum metallic conductivity[7]. While many such properties might prove instrumental if graphene is to be used in future technological applications in the ever pressing demand for miniaturization in electronics, the latter is actually a strong deterrent: it hinders the pinching off of the charge flow and the creation of quantum point contacts. In addition, graphene has a gapless spectrum with linearly dispersing, Dirac-like, excitations[8,9]. Although a gap can be induced by means of quantum confinement in the form of nanoribbons[10] and quantum dots[11], these "paper-cutting" techniques are prone to edge roughness, which has detrimental effects on the electronic properties. Hence, a route to induce a robust, *clean*, bulk spectral gap in graphene is still much in wanting.

In this paper we inquire whether the seemingly independent aspects of mechanical response and electronic properties can be brought together with profit in the context of a tunable electronic structure. Motivated by recent experiments showing that reversible and controlled strain can be produced in graphene with measurable effects[12,13], we theoretically explore the effect of strain in the electronic structure of graphene within a tight-binding approach. Our calculations show that, in the absence of electron-electron interactions, a gap can be opened in a pure tight binding model of graphene for deformations beyond 20%. This gap opening is not a consequence of a broken sublattice symmetry but due to level crossing. The magnitude of this effect depends on the direction of applied tension, so that strain along a zig-zag direction is most effective in overcoming the gap threshold, whereas deformations along an armchair direction do not induce a gap. Unfortunately, such large threshold deformations render strain an ineffective means to achieve a bulk gapped spectrum in graphene. We discuss alternate means to impact transport and electronic structure using local strain profiles.

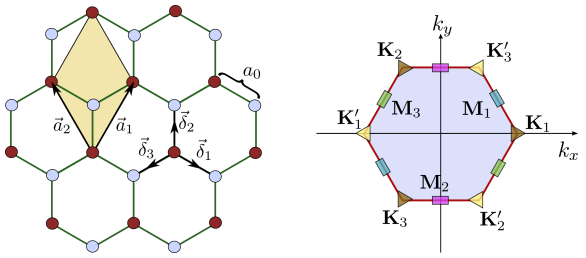
I. MODEL

We consider that electron dynamics of electrons hopping in the honeycomb lattice is governed by the nearest



(a)

FIG. 1: (Color online) (a) Tension geometry considered in the text. The zig-zag direction of the honeycomb lattice is always parallel to the axis Ox.



(a) (b)

FIG. 2: (Color online) (a) Honeycomb lattice geometry. The vectors $\boldsymbol{\delta}_1 = a(\frac{\sqrt{3}}{2}, -\frac{1}{2})$, $\boldsymbol{\delta}_2 = a(0,1)$ $\boldsymbol{\delta}_3 = a(-\frac{\sqrt{3}}{2}, -\frac{1}{2})$ connect A-sites (red/dark) to their B-site (blue/light) neighbors. (b) The first Brillouin zone of undeformed graphene, with its points of high symmetry.

neighbor tight-binding Hamiltonian

$$H = \sum_{\boldsymbol{R},\boldsymbol{\delta}} t(\boldsymbol{R},\boldsymbol{\delta}) a^\dagger(\boldsymbol{R}) b(\boldsymbol{R}+\boldsymbol{\delta}) + \text{H. c.}\,. \tag{1}$$

Here $\boldsymbol{R}$ denotes a position on the Bravais lattice, and $\boldsymbol{\delta}$ connects the site $\boldsymbol{R}$ to its neighbors; $a(\boldsymbol{R})$ and $b(\boldsymbol{R})$ are the field operators in sublattices A and B. The first thing to emphasize is that, under general stress conditions, the hopping $t(\boldsymbol{R},\boldsymbol{\delta})$ will be generally different among different neighbors. We are interested in the elastic response, for which deformations are affine. This means that even though the hoppings from a given atom to its neighbors can be all different, they will be the same for every atom. Therefore, as depicted in Fig. 2(a), we need only to consider three distinct hoppings: $t_1 = t(\boldsymbol{\delta}_1)$, $t_2 = t(\boldsymbol{\delta}_2)$, and $t_3 = t(\boldsymbol{\delta}_3)$. The relaxed equilibrium value for $t_i = t(\boldsymbol{\delta}_i)$ is $t_0 \approx 2.7$ eV[9]. Our goal is to investigate the changes that strain induces in these hoppings, and what impact they have in the resulting electronic structure.

Throughout this paper we shall use the C–C equilibrium distance, $a_0 = 1.42$ Å, as unit of length, and will frequently use t_0 as unit of energy.

II. ANALYSIS OF STRAIN

We are interested in uniform planar tension situations, like the one illustrated in Fig. 1(a): the graphene sheet is uniformly stretched (or compressed) along a prescribed direction. The fixed Cartesian system is chosen in a way that Ox always coincides with the zig-zag direction of the lattice. In these coordinates the tension, $\boldsymbol{T}$, reads $\boldsymbol{T} = T\cos(\theta)\,\boldsymbol{e}_x + T\sin(\theta)\,\boldsymbol{e}_y$.

As for any solid, the generalized Hooke's law relating stress, τ_{ij} and strain ε_{ij} has the form

$$\tau_{ij} = C_{ijkl}\,\varepsilon_{kl}\,, \quad \varepsilon_{ij} = S_{ijkl}\,\tau_{kl} \tag{2}$$

where $C_{ijkl}\,(S_{ijkl})$ are the components of the stiffness (compliance) tensor. Since we address only states of planar stress, we resort to the 2-dimensional reduction of the stress and strain tensors. In general the components C_{ijkl} depend on the particular choice of the Cartesian axes. Incidentally, for an hexagonal system under planar stress in the basal plane, the elastic components are independent of the coordinate system. This means that graphene is elastically isotropic[14].

The analysis of strain is straightforward in the principal system $Ox'y'$ where we simply have $\boldsymbol{T} = T\boldsymbol{e}_{x'}$:

$$\varepsilon'_{ij} = S_{ijkl}\tau'_{kl} = T\,S_{ijkl}\delta_{kx}\delta_{lx} = T\,S_{ijxx} \tag{3}$$

Given that only five compliances are independent in graphite (viz., S_{xxyy}, S_{xxyy}, S_{xxzz}, S_{zzzz}, S_{yzyz})[15], it follows that the only non-zero deformations are

$$\varepsilon'_{xx} = T\,S_{xxxx}\,,\ \varepsilon'_{yy} = T\,S_{xxyy}\,, \tag{4}$$

which represent the longitudinal deformation and Poisson's transverse contraction. If we designate the tensile strain by $\varepsilon = T\,S_{xxxx}$, the strain tensor can be written in terms of Poisson's ratio, $\sigma = -S_{xxyy}/S_{xxxx}$:

$$\boldsymbol{\varepsilon}' = \varepsilon \begin{pmatrix} 1 & 0 \\ 0 & -\sigma \end{pmatrix}. \tag{5}$$

This form shows that graphene responds as an isotropic elastic medium. For Poisson's ratio we use the value known for graphite: $\sigma = 0.165$[15]. It should be mentioned that when stress is induced in graphene by mechanically acting on the substrate (i.e. when graphene is adhering to the top of a substrate and the latter is put under tension, as is done in Ref. 12), the relevant parameter is in fact the tensile strain, ε, rather than the tension T[16]. For this reason, we treat ε as the tunable parameter. Since the lattice is oriented with respect to the axes Oxy, the stress tensor needs to be rotated to extract information about bond deformations. The strain tensor in the lattice coordinate system reads

$$\boldsymbol{\varepsilon} = \varepsilon \begin{pmatrix} \cos^2\theta - \sigma\sin^2\theta & (1+\sigma)\cos\theta\sin\theta \\ (1+\sigma)\cos\theta\sin\theta & \sin^2\theta - \sigma\cos^2\theta \end{pmatrix}. \tag{6}$$

III. BOND DEFORMATIONS

If $\boldsymbol{v}^0$ represents a general vector in the undeformed graphene plane, its deformed counterpart is given, to leading order, by the transformation

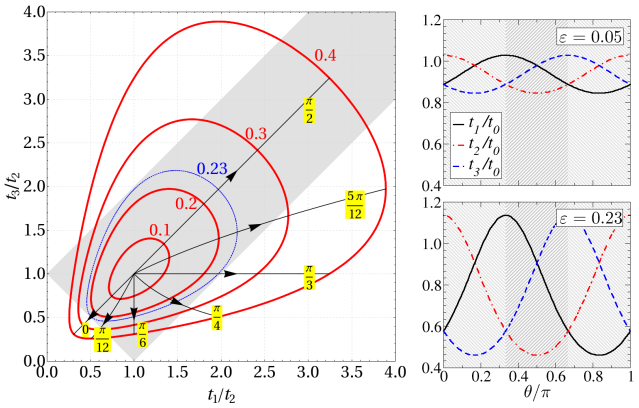
$$\boldsymbol{v} = (\mathbf{1} + \boldsymbol{\varepsilon})\cdot\boldsymbol{v}^0\,. \tag{7}$$

Especially important are the deformations of the nearest-neighbor bond distances. Knowing ε_{ij} one readily obtains the deformed bond vectors using (7). The new bond lengths are then given by

$$|\boldsymbol{\delta}_1| = 1 + \tfrac{3}{4}\varepsilon_{11} - \tfrac{\sqrt{3}}{2}\varepsilon_{12} + \tfrac{1}{4}\varepsilon_{22} \tag{8a}$$

$$|\boldsymbol{\delta}_2| = 1 + \varepsilon_{22} \tag{8b}$$

$$|\boldsymbol{\delta}_3| = 1 + \tfrac{3}{4}\varepsilon_{11} + \tfrac{\sqrt{3}}{2}\varepsilon_{12} + \tfrac{1}{4}\varepsilon_{22} \tag{8c}$$



(a) (b)

FIG. 3: (Color online) (a) Plot of t_1/t_2 vs t_3/t_2 as a function of strain, ε, and θ. Closed lines are iso-strain curves, and arrowed lines correspond to the trajectory of the point $(t_1/t_2, t_3/t_2)$ as ε increases, calculated at constant angle. The graph is symmetric under reflection on both axes. In the shaded area the spectrum is gapless. The blue iso-strain line ($\varepsilon \approx 0.23$) corresponds to the gap threshold. In panel (b) we show the angular dependence of $t_{1,2,3}$ for $\varepsilon = 0.05$ and $\varepsilon = 0.23$.

Of particular interest are the cases $\theta = 0$ and $\theta = \pi/2$ since they correspond to tension along the zig-zag ($\mathcal{Z}$) and armchair ($\mathcal{A}$) directions:

$$\mathcal{Z}: \quad |\boldsymbol{\delta}_1| = |\boldsymbol{\delta}_3| = 1 + \tfrac{3}{4}\varepsilon - \tfrac{1}{4}\varepsilon\sigma\,, \; |\boldsymbol{\delta}_2| = 1 - \varepsilon\sigma \tag{9a}$$

$$\mathcal{A}: \quad |\boldsymbol{\delta}_1| = |\boldsymbol{\delta}_3| = 1 + \tfrac{1}{4}\varepsilon - \tfrac{3}{4}\varepsilon\sigma\,, \; |\boldsymbol{\delta}_2| = 1 + \varepsilon \tag{9b}$$

The modification of these distances distorts the reciprocal lattice as well, and the positions of the high-symmetry points shown in Fig. 2(b) are shifted. The primitive vectors of the reciprocal space are denoted by $\boldsymbol{b}_{1,2}$, and, in leading order, change according to

$$\boldsymbol{b}_1 \approx \frac{2\pi}{\sqrt{3}}\left(1 - \varepsilon_{11} - \frac{\varepsilon_{12}}{\sqrt{3}}; \frac{1}{\sqrt{3}} - \varepsilon_{12} - \frac{\varepsilon_{22}}{\sqrt{3}}\right), \tag{10a}$$

$$\boldsymbol{b}_2 \approx \frac{2\pi}{\sqrt{3}}\left(-1 + \varepsilon_{11} - \frac{\varepsilon_{12}}{\sqrt{3}}; \frac{1}{\sqrt{3}} + \varepsilon_{12} - \frac{\varepsilon_{22}}{\sqrt{3}}\right). \tag{10b}$$

Most importantly, the symmetry point $\boldsymbol{K} = (\frac{4\pi}{3\sqrt{3}}, 0)$ (that coincides with the Fermi point in the undoped, equilibrium situation, and chosen here for definiteness) moves to the new position

$$\boldsymbol{K} \approx \frac{4\pi}{3\sqrt{3}}\left(1 - \frac{\varepsilon_{11}}{2} - \frac{\varepsilon_{22}}{2}; -2\varepsilon_{12}\right) \tag{11}$$

for a general deformation, and in leading order in strain. For uniaxial tension this reduces to

$$\boldsymbol{K} \approx \frac{4\pi}{3\sqrt{3}}\left(1 - \frac{\varepsilon(1-\sigma)}{2}; -\varepsilon(1+\sigma)\,\sin[2\theta]\right). \tag{12}$$

The factor of 2θ means that the shift is the same for the $\mathcal{A}$ and $\mathcal{Z}$ directions, in leading order. These general results will be important for our subsequent discussion.

IV. HOPPING RENORMALIZATION

The change in bond lengths (8) leads to different hopping amplitudes among neighboring sites. In the Slater-Koster scheme[17], the new hoppings can be obtained from the dependence of the integral $V_{pp\pi}$ on the inter-orbital distance. Unfortunately determining such dependence with accuracy is not a trivial matter. Many authors resort to Harrison's flyleaf expression which suggests that $V_{pp\pi}(l) \propto 1/l^2$[18]. However this is questionable, insofar as such dependence is meaningful only in matching the tight-binding and free electron dispersions of simple systems in equilibrium (beyond the equilibrium distance such dependence is unwarranted[18]). It is indeed known that such functional form fails away from the equilibrium distance[19], and a more reasonable assumption is an exponential decay[20]. In line with this we assume that, in graphene

$$V_{pp\pi}(l) = t_0 e^{-3.37(l/a_0 - 1)}\,, \tag{13}$$

where the rate of decay is extracted from the experimental result $dV_{pp\pi}/dl = -6.4$ eV/Å[21]. As a consistency check, we point out that, according to Eq. (13), the next-nearest neighbor hopping (t') would have the value $V_{pp\pi}(\sqrt{3}a_0) = 0.23$ eV, which tallies with existing estimates of t' in graphene[9].

V. GAP THRESHOLD

The bandstructure of Eq. (1) with arbitrary hoppings t_1, t_2, t_3 is given by

$$E(k_x, k_y) = \pm\left|t_2 + t_3\, e^{-i\boldsymbol{k}.\boldsymbol{a}_1} + t_1\, e^{-i\boldsymbol{k}.\boldsymbol{a}_2}\right|. \tag{14}$$

Here both t_α and the primitive vectors $\boldsymbol{a}_\alpha$ (see Fig. 2(a) for the definition of the vectors $\boldsymbol{a}_\alpha$) change under strain: the hoppings change as per Eqs. (13,8), and the primitive vectors as per Eq. (7). This generalized dispersion has been previously discussed in Refs. 22,23, under the assumption that only the hopping elements change, without lattice deformation. It was found that the gapless spectrum is robust, and that a gap can only appear under anisotropy in excess of 100% in one of the hoppings. More specifically, the spectrum remains gapless as long as the condition

$$\left|\frac{|t_1|}{|t_2|} - 1\right| \le \frac{|t_3|}{|t_2|} \le \left|\frac{|t_1|}{|t_2|} + 1\right| \tag{15}$$

is in effect. This condition corresponds to the shaded area in Fig. 3(a). Using the results in eqs. (6, 8, 13) we have mapped the evolution of the hoppings with ε and θ. This allows us to identify the range of parameters that violate (15), and to obtain the threshold for gap opening. For a given θ, we follow the trajectory of the point $(t_1/t_2,\, t_3/t_2)$ as strain grows, starting from the isotropic point at $\varepsilon = 0$. The result is one of the arrowed curves in Fig. 3(a). The value of ε at which this curve leaves the

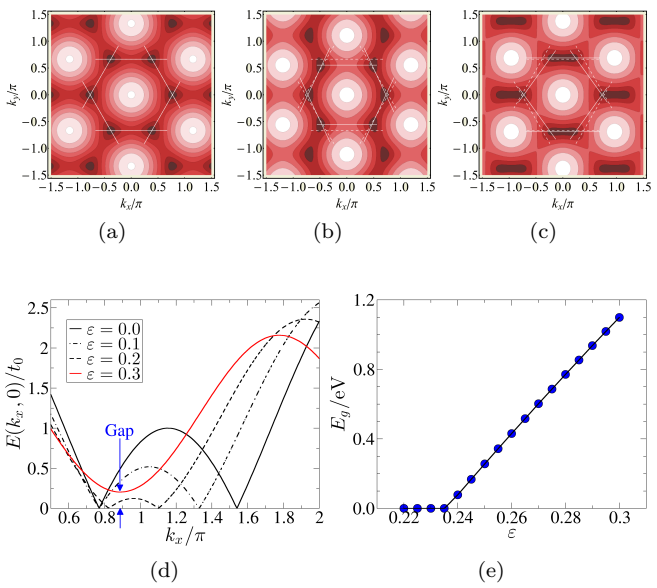


FIG. 4: (Color online) Top row shows density plots of the energy dispersion, $E(k_x, k_y)$, for $\{\varepsilon = 0, \theta = 0\}$ (a), $\{\varepsilon = 0.2, \theta = \pi/2\}$ (b), and $\{\varepsilon = 0.2, \theta = 0\}$ (c). In these plots, the central white dashed lines represent the boundary of the first BZ of the undeformed lattice, while the solid white lines mark the boundaries of the BZ for the deformed lattice. In (d) we have a cut of (c) along $k_y = 0$, showing the merging of the Dirac cones as strain increases, and the ultimate appearance of the gap. In panel (e) we compare the gap given by Eq. (18) (line) with the result obtained from direct minimization of the energy in the full BZ (dots).

shaded area corresponds to the gap threshold for that particular angle. From such procedure, summarized in Fig. 3(a), we conclude that: (i) the gap threshold is at $\varepsilon \approx 0.23$ ($\sim 20\%$); (ii) the behavior of the system is periodic in θ with period $\pi/3$, in accord with the symmetry of the lattice; (iii) tension along the zig-zag direction ($\theta = 0, \pi/3, \dots$) is more effective in overcoming the gap threshold; (iv) tension along the armchair direction never generates a gap.

The two panels of Fig. 3(b) contain plots of the individual t_α for two particular values of strain. It is clear that, for deformations along the $\mathcal{Z}$ direction, the highest relative change occurs along the zig-zag bonds ($t_{1,3}$), and conversely for deformations along the $\mathcal{A}$ direction. This could have also been anticipated from Eqs. (9) and the smallness of σ.

VI. CRITICAL GAP

The fact that the isotropic point $(1, 1)$ in Fig. 3(a) is surrounded by an appreciable shaded area, means that the gapless situation is robust, and the emergence of the gap requires a critical strain. The physical effect behind such critical gap lies in the fact that, under strain, the Dirac cones drift away from the points $\boldsymbol{K}$, $\boldsymbol{K}'$ in the Brillouin zone (BZ). Before we proceed, it is pertinent to advance a crucial detail: in a deformed lattice, the Dirac points (i.e. the positions in the BZ where conduction and valence bands touch conically) and the symmetry points $\boldsymbol{K}_i$ do not coincide. In what follows we shall distinguish them explicitly.

To be more definite, we examine the position of the minimum energy[24] for the bands obtained from Eq. (14), which can be done exactly if we assume that the lattice remains undeformed. Due to the particle-hole symmetry, we minimize $E(\boldsymbol{k})^2$. Let us assume that $t_1 = t_3 \neq t_2$, which applies for tension along either zig-zag or armchair directions. In that case the spectrum has minima at exactly

$$\boldsymbol{k}_{\min} = \left(\pm \frac{2}{\sqrt{3}} \arccos\left[-\frac{t_2}{2t_1} \right]; 0 \right), \tag{16}$$

and all symmetry related points. The $\pm$ sign refers to one possible choice for the two inequivalent valleys. In addition to these local minima, that correspond to the Dirac points, the dispersion has saddle points at

$$\boldsymbol{k} = \left(\frac{\pi}{\sqrt{3}}; \frac{\pi}{3} \right), \boldsymbol{k} = \left(0; \frac{2\pi}{3} \right), \boldsymbol{k} = \left(\frac{\pi}{\sqrt{3}}; -\frac{\pi}{3} \right) \tag{17}$$

(and all symmetry related points). These are just the points $\boldsymbol{M}_1$, $\boldsymbol{M}_2$, $\boldsymbol{M}_3$ shown in Fig. 2(b) and their position is independent of t_i[25]. The values of energy at these points are $E(\boldsymbol{M}_1) = |t_1 + t_2 - t_3|$, $E(\boldsymbol{M}_2) = |-t_1 + t_2 + t_3|$ and $E(\boldsymbol{M}_3) = |t_1 - t_2 + t_3|$.

The result in Eq. (16) shows that the Dirac points drift away from the $\boldsymbol{K}$ point, and the direction of that drift is dictated by the relative variations in t_i. For example, for uniaxial tension along the $\mathcal{Z}$ we have $t_2 > t_1 = t_3$, and therefore the minimum of energy moves to the right (left) of $\boldsymbol{K_1}$ ($\boldsymbol{K_1'}$) [cfr. Fig. 2(b)]. This means that the inequivalent Dirac points move toward each other, and will clearly meet when $2t_1 = t_2$. They meet precisely at the position of the saddle point $\boldsymbol{M}_2$. Throughout this process, the dispersion remains linear along the two orthogonal directions, albeit with different Fermi velocities. If the hoppings change further so that $2t_1 > t_2$, the solution (16) is no longer valid, and the minimum lies always at $\boldsymbol{M}_2$. Since the energy at this saddle point is given exactly by $E(\boldsymbol{M}_2) = |2t_1 - t_2|$, the system becomes gapped, with a gap $\Delta = 2|2t_1 - t_2|$. Moreover, the dispersion becomes peculiar in that it remains linear along one direction (the y direction in this example) and quadratic along the other. The topological structure is also modified since the two inequivalent Dirac cones have merged[26].

These considerations assume that the hoppings can change but the lattice remains undeformed. Under a real deformation both lattice and hoppings are affected. The lattice deformation will distort the BZ but will not affect the aspects discussed above. This can be clearly seen from inspection of the energy dispersions plotted in

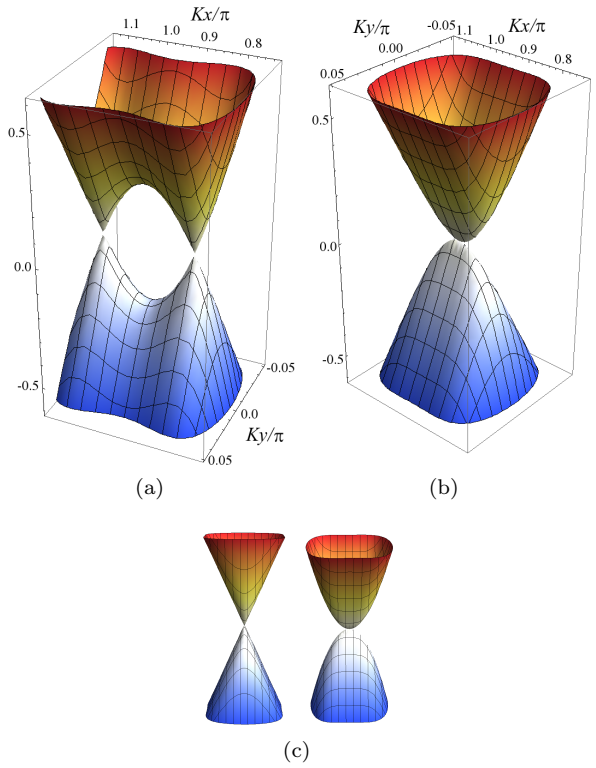


FIG. 5: (Color online) Closeup of the energy dispersion $E(\boldsymbol{k})$ in the vicinity of the Dirac points. Panel (a) shows a pre-critical situation (in which the two cones persist) for a strain of $\varepsilon = 0.2$ along the zig-zag ($\theta = 0$) direction. Notice how the saddle point approaches zero energy with increasing strain. In (b) we show the bandstructure at precisely the critical strain for which the two Dirac cones meet. The dispersion is quadratic along k_x (the direction of strain) but remains linear along k_y. This can be seen in (c) where we show the critical dispersion viewed from the k_x and k_y axes, respectively.

Fig. 4(a-c). The plotted dispersions include the deformation of the BZ and the change in the hoppings, simultaneously. For strain along the $\mathcal{A}$ direction the nonequivalent Dirac cones move in opposite directions and never meet [Fig. 4(b)]. However, if the deformation is along the $\mathcal{Z}$ direction, the cones always approach each other [Fig. 4(c)], and will eventually merge. This merging is seen in detail in Fig. 4(d) where a cut along $k_y = 0$ is presented to show the emergence of the gap beyond the threshold deformation. For tension along an arbitrary direction (except armchair) the cones always merge, the $\mathcal{Z}$direction being the optimal orientation, requiring less strain [cfr. Fig. 3(a)]. Precisely at the critical point, the dispersion is linear along k_x and quadratic along k_y, as shown in Fig. 5. This modification in the dispersion along one of the Cartesian directions has peculiar implications for the DOS and Landau level quantization[27].

The gap is a result of this Dirac cone merging process, and the origin of the high critical strain is now clear: one needs to deform enough to bring the two Dirac points to

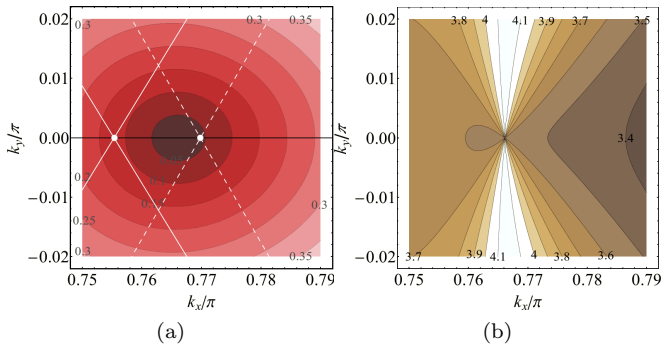


FIG. 6: (Color online) (a) A close-up of the energy dispersion close to its minimum, for tension along $\theta = 0$ and $\varepsilon = 0.05$. The solid white lines show the intersection of the Bragg planes that define the boundary of the first BZ in the deformed lattice, while the dashed white lines represent the same boundary es in equilibrium. It is clear that the Dirac point lies neither at $\boldsymbol{K}$, nor at its deformed counterpart. The energy contours are labeled in eV. (b) A contour plot of the absolute value of the Fermi velocity, $\hbar v_F = \nabla_{\boldsymbol{k}} E(\boldsymbol{k})$ for the same region shown in (a).

coincidence. This agrees with the existing understanding that the gapless Dirac spectrum in graphene is robust (topologically protected) with respect to small perturbations.

For strain along $\theta = 0$, as discussed above, the gap is conveniently given by

$$E_g(\varepsilon) = 2\left|2t_1(\varepsilon) - t_2(\varepsilon)\right|\theta(t_2 - 2t_1)\,. \qquad (18)$$

An example of the strain dependence of E_g can be seen in Fig. 4(e). In it we see the agreement between the gap given by Eq. (18) and the value extracted from a direct minimization of $E(k_x, k_y)$ in the full (deformed) BZ.

From Fig. 4(b) one can see that pulling along an armchair direction imparts 1D-like features to the system: the dispersion becomes highly anisotropic. This is explained on account of the results plotted in Fig. 3(b) which show that stress along $\mathcal{A}$ tends to weaken one bond only. In extreme cases, the weak bond can be highly suppressed leaving only a set of 1D chains[28]. This means that strain along certain directions can be used as a means to induce preferred anisotropy in electric transport. In contrast, pulling along a zig-zag direction tends to dimerize the system for large deformations, which ultimately explains the appearance of the gap in this case.

VII. POSITION OF THE DIRAC POINT

The fact that there are two concurrent effects determining the changes in the bandstructure (viz. the lattice distortion itself, and the modification in the nearest-neighbor hoppings) means that the position of the minimum of energy *does not coincide with the symmetry points of the deformed BZ*. This is documented in

Fig. 6(a) where we provide a close-up of the energy dispersion close to the Dirac point. This should be clear from the foregoing discussion on the merging of the Dirac points. In any case we want to stress this effect and illustrate it by analyzing small perturbations with respect to the undeformed situation. For definiteness let us focus again in the case $t_1 = t_3$. The position of the new $\boldsymbol{K}$ was given already in eqs. (11,12). The position of the Dirac point is given by eq. (16) when only the hoppings change, but not the lattice. For a small perturbation ($t_2 \approx t_1$) the result (16) reduces to[29]

$$\boldsymbol{k}_{\min} \approx \pm\left(\frac{4\pi}{3\sqrt{3}} + 2\frac{t_2 - t_1}{3t_1}; 0\right). \tag{19}$$

One can calculate the correction to this result simultaneously accounting for the lattice deformation. But the lengthy expression that results is less important than the qualitative effect: the corrections to the expression (19) depend on the specific details of the variation of t_i with distance. Consequently, the Dirac point and the $\boldsymbol{K}$ point of the deformed lattice do not coincide in general. The equilibrium situation, in which they coincide, is a very particular case.

In fact, even assuming a simple lattice distortion that does not change the hoppings will move the Dirac point away from the symmetry point of the resulting lattice. This can be seen from a low energy expansion of (14) putting $t_i = t$. The position of the Dirac point $\boldsymbol{K}_1$ in such case moves to

$$\boldsymbol{k}_{\min} \approx \left(\frac{4\pi}{3\sqrt{3}}(1 - \varepsilon_{11}); -\frac{4\pi}{3\sqrt{3}}\varepsilon_{12}\right), \tag{20}$$

which is clearly different from (11). This fact is of critical relevance when interpreting results of similar calculations obtained *ab-initio*, as will be discussed below.

The fact that the Dirac point drifts from the corner of the BZ means that there are no longer 3 equivalent pairs of points in the first BZ for the neutral system, but only one pair of non-equivalent points in general (in other words, in the undoped and undeformed lattice the Fermi surface is distributed among the 6 degenerate K points in the boundary of the BZ, whereas for a general deformation we have only two within the rst BZ). In the situation shown in Fig. 6(a), for example, the Dirac point shown in the figure lies outside the first Brillouin zone. The one inside the first BZ is actually the (equivalent) Dirac point that moved away from $\boldsymbol{K}_2$ (or $\boldsymbol{K}_3$), in the notation of Fig. 2(b).

VIII. DISCUSSION

We have seen that, within the tight-binding Hamiltonian written in Eq. (1), uniform tension can induce a bulk spectral gap in graphene. However, at least within a non-interacting tight-binding approach, the gap threshold is very difficult to overcome, if at all possible. Since a tensional strain in excess of 20% is required to observe such feature, several comments are in order.

A. On the approximations employed

We start by noticing that in our calculation we kept only the lowest order terms in ε. In addition, although strain magnitudes of $\sim 20\%$ are not unreasonable, graphene is expected to be in the non-linear elastic regime at those deformations[3]. Therefore, non-linear corrections can be relevant at the quantitative level in the vicinity of the threshold.

Notwithstanding, our main result is robust: no gap can be opened under planar tension situations, except in highly strained situations. This conclusion does not depend on having taken a linear approximation insofar as it should be valid up to deformations in the range of 5-10%.

With respect to our tight-binding parametrization including only nearest neighbor hopping, we should mention that Kishigi *et al.*have shown that inclusion of next-nearest neighbor terms (t') can, alone, generate a gap[30]. But this requires a very specific deformation of the lattice, unlikely to occur under simple tension. The presence of t' can also lead to other effects, like tilted Dirac cones as discussed in Ref. 31.

It is expected that the planar arrangement of carbon atoms in freely hanging graphene should become unstable with respect to a buckled or rippled configuration, or even experience mechanical failure for moderate to high tension. The presence of a substrate should provide more stability for the planar distribution of the carbon atoms. In fact, a recent experiment published during revision of this manuscript[32] shows that reversible strain of the order of 18% can be induced in graphene deposited on flexible plastic substrates.

B. On related *ab-initio* calculations

Secondly, some *ab-initio* calculations seem to show that a gap is present in graphene for arbitrarily small tensions[12,33]. But these reports have some conflicting details. For example there is an order of magnitude discrepancy between the gap predicted in these two references for 1% strain. In addition, Ref. 33 claims their *ab-initio* result agrees with the bandstructure (14) after a suitable choice of hoppings. As we showed above this cannot be the case, since there is always a (large) threshold for the appearance of the gap. Consequently, further clarification regarding *ab-initio* under strain is desired.

One issue that requires special attention in interpreting density functional theory (DFT) calculations of graphene's bandstructure under strain is the shift of the Dirac point. As we stressed earlier, when graphene is strained the Dirac point (position of the energy minimum) does not lie at any symmetry point of the lat-

tice. This is paramount because DFT calculations of the bandstructure rely on a preexisting mesh in reciprocal space, at whose points the bandstructure is sampled. These meshes normally include points along high symmetry lines of the BZ. But in the current problem, the use of such a traditional mesh will not be particularly useful to distinguish between a gapped and gappless situation. Since the Fermi surface of undoped graphene is a single point, unless the sampling mesh includes that precise point, one will always obtain a gap in the resulting bandstructure.

Most recently, we became aware of two new developments from the *ab-initio* front, that shed the light needed to interpret the earlier calculations mentioned above. One of them[34] is a revision of the DFT calculations presented in Ref. 12. In this latter work it is shown that, upon careful analysis, the DFT calculation shows no gap under uniaxial deformations up to $\sim 20\%$. In fact the authors mention explicitly that the shift of the Dirac point from the high symmetry point mislead the authors in their initial interpretation of the bandstructure. In another preprint[35], independent authors show that their DFT calculations reveal, again, no gap for deformations of the order of 10% in either the $\mathcal{Z}$ or $\mathcal{A}$ directions. These subsequent developments confirm our prediction that only excessive planar deformations are able to engender a bulk spectral gap in graphene.

C. Anisotropic Transport

Several effects of tensional strain are clear from our results. Tension leads to one-dimensionalization of transport in graphene by weakening preferential bonds: transport should certainly be anisotropic, even for small tensions. One example of that is seen in Fig. 6(a) where a strain of 5% visibly deforms the Fermi surface. Fig. 6(b), where the Fermi velocity is plotted for the same region in the BZ, further shows that, for the chosen tension direction, the Fermi surface is not quite elliptical but slightly oval, in a reminiscence of the trigonal warping effects.

The anisotropy in the Fermi velocity can become quite large, as shown in Fig. 7. There we plot the ratio $v_{F(\max)}/v_{F(\min)}$ for $E_F = 50$ meV. As can be seen in the cuts of Fig. 4(d), near the critical strain the Fermi level may touch the van Hove singularity (midpoint between the two cones) where $v_F = 0$ along one direction, which leads to formal divergence of the ratio between the maximum and minimum Fermi velocities.

The Fermi surface anisotropy has been captured in transport experiments that reveal a considerable anisotropy in the resistivities parallel (R_{xx}) and perpendicular (R_{yy}) to the tension direction[32]. The authors of Reference 32 report in their Fig. 4c resistivity anisotropies of up to one order of magnitude at $\sim 19\%$ strain. We can make a simple estimate of the anisotropies expected in the light of our results for the deformed bandstructure. For that we follow a Boltzmann approach to the relaxation time and DC conductivity. As is usually the case, the relevant electron states are the ones lying in a narrow vicinity of the Fermi surface. On account of the Fermi surface anisotropy, we can take the Fermi velocities in the direction of the electric field only. For example, in the situation shown in Fig. 6(a) for uniaxial strain along Ox, the relevant v_F's determining R_{xx} and R_{yy} will be the ones along the major and minor axes, respectively.

For the purposes of our estimate, we take the Boltzmann longitudinal conductivity for scattering out of unscreened charged impurities of valence Z and concentration n_i[36], given by

$$\sigma = \frac{2e^2}{h}\frac{\pi\hbar^2 v_F^2 n}{Z^2 e^2 n_i}\,, \tag{21}$$

and follow the reasoning above: replacing $v_F \to \boldsymbol{v}_F.\boldsymbol{u}_E$, where $\boldsymbol{u}_E$ is the direction of the electric field in each case (parallel or perpendicular to the tension direction). We immediately see that this estimate leads to a resistance anisotropy of[37]

$$\frac{R_{xx}}{R_{yy}} \approx \left(\frac{v_{F(\max)}}{v_{F(\min)}}\right)^2. \tag{22}$$

For the maximum strain used in the experiment ($\sim 19\%$) our plot in Fig. 6(b) yields a ratio of 2.8, which, per (22), corresponds to a resistance anisotropy of roughly 8 fold, consistent with the measured anisotropy.

Our results apply to exfoliated and epitaxial graphene alike. As matters currently stand, it is perhaps more relevant in the context of the latter, since graphene grown epitaxialy on SiC is almost always under strain[38]. The strained configurations are imposed by the lattice mismatch with the substrate, and can be controlled by changing the growth and annealing conditions[39]. For these systems, the relaxed starting configuration is already deformed.

Lastly, it is important to point out that, even though a spectral gap seems to require extreme strain, one can generate a *transport* gap by means of local, small, deformations. It has been shown in Refs. 40,41 that tunneling across a locally strained region is highly suppressed, and leads to a transport gap (i.e., a suppression of electrical conductivity) at small densities, even in the absence of a bulk spectral gap.

IX. CONCLUSIONS

Within a non-interacting, nearest-neighbor tight-binding approach, we have shown that opening a spectral gap in strained graphene requires deformations of the order of 20%. This result is confirmed by the most recent *ab-initio* calculations. Such an extreme strain is required on account of the stability of the Dirac points in graphene, that renders the spectrum gappless unless

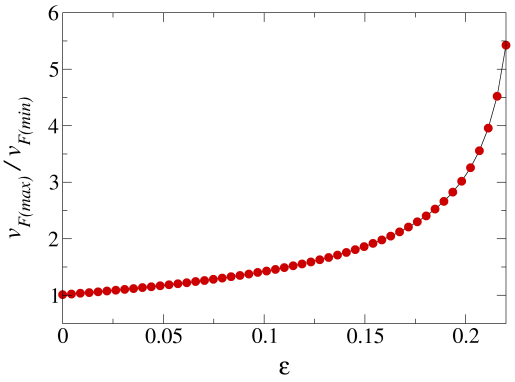


FIG. 7: (Color online) Anisotropy in the Fermi velocity, as a function of strain for a Fermi energy of 50meV. The vertical axis shows the ratio of the maximum to the minimum values of v_F in the entire Fermi surface.

the two inequivalent Dirac points merge. The merging requires substantial anisotropy in the hopping integrals, only achieved under high strain. General features of strained graphene are an anisotropic Fermi surface, anisotropic Fermi velocities, and the drift of the Dirac points away from the high symmetry points of the lattice.

Uniform planar stain appears to be an unlikely candidate to induce a bulk gap in graphene. Nevertheless, strain (local or uniform) can be an effective means of tuning the electronic structure and transport characteristics of graphene devices. Even if the bulk gap turns out to be challenging in practice, local strain could be used as a way to mechanically pinch off current flow.

Acknowledgments

We thank enlightening discussions with Y. P. Feng, A. K. Geim, A. Heinz, Y. Lu, Z. Ni, Z. X. Shen, and T. Yu. AHCN acknowledges the partial support of the U.S. Department of Energy under the grant DE-FG02-08ER46512. VMP is supported by FCT via SFRH/BPD/27182/2006 and PTDC/FIS/64404/2006.

[1] M.-F. Yu, O. Lourie, M. J. Dyer, K. Moloni, T. F. Kelly, and R. S. Ruoff, Science **287**, 637 (2000).
[2] C. Lee, X. Wei, J. W. Kysar, and J. Hone, Science **321**, 385 (2008).
[3] F. Liu, P. Ming, and J. Li, Phys. Rev. B **76**, 064120 (2007).
[4] A. K. Geim and K. S. Novoselov, Nat. Mat. **6**, 183 (2007).
[5] K. S. Novoselov, A. K. Geim, S. V. Morozov, D. Jiang, Y. Zhang, S. V. Dubonos, I. V. Grigorieva, and A. A. Firsov, Science **306**, 666 (2004).
[6] T. Ando and T. Nakanishi, J. Phys. Soc. Jpn. **67**, 1704 (1998).
[7] K. S. Novoselov, A. K. Geim, S. V. Morozov, D. Jiang, M. I. Katsnelson, I. V. Grigorieva, S. V. Dubonos, and A. A. Firsov, Nature **438**, 197 (2005).
[8] P. R. Wallace, Phys. Rev. Lett. **71**, 622 (1949).
[9] A. H. Castro Neto, F. Guinea, N. M. R. Peres, K. S. Novoselov, and A. K. Geim, Rev. Mod. Phys. **81**, 109 (2009).
[10] M. Y. Han, B. Özyilmaz, Y. Zhang, and P. Kim, Phys. Rev. Lett. **98**, 206805 (2007).
[11] L. A. Ponomarenko, F. Schedin, M. I. Katsnelson, R. Yang, E. W. Hill, K. S. Novoselov, and A. K. Geim, Science **320**, 356 (2008).
[12] Z. Ni, T. Yu, Y. H. Lu, Y. Y. Wang, Y. P. Feng, and Z. X. Shen, ACS Nano **2**, 2301 (2008).
[13] Z. Ni, H. M. Wang, Y. Ma, J. Kasim, Y. H. Wu, and Z. X. Shen, ACS Nano **2**, 1033 (2008).
[14] L. D. Landau and E. M. Lifshitz, *Theory of Elasticity* (Pergamon, 1986), 3rd ed.
[15] L. Blakslee, D. G. Proctor, E. J. Seldin, G. B. Stence, and T. Wen, J. Appl. Phys. **41**, 3373 (1970).
[16] In this case the relation between strain and stress is given by the material parameters of the substrate, rather than the intrinsic elastic parameters for graphene.
[17] J. C. Slater and G. F. Koster, Phys. Rev. **94**, 1498 (1954).
[18] W. A. Harrison, *Elementary Electronic Structure* (World Scientific, 1999), ISBN 981–023895-9.
[19] G. Grosso and C. Piermarocchi, Phys. Rev. B **51**, 16772 (1995).
[20] D. A. Papaconstantopoulos, M. J. Mehl, S. C. Erwin, and M. R. Pederson, in *Tight-Binding Approach to Computational Materials Science*, edited by P. Turchi, A. Gonis, and L. Colombo (Materials Research Society, Pittsburgh, 1998), p. 221.
[21] A. H. Castro Neto and F. Guinea, Phys. Rev. B **75**, 045404 (2007).
[22] B. Wunsch, F. Guinea, and F. Sols, New J. Phys. **10**, 103027 (2008).
[23] Y. Hasegawa, R. Konno, H. Nakano, and M. Kohmoto, Phys. Rev. B **74**, 033413 (2006).
[24] By "position of the minimum energy" we mean the position of the Dirac points (or valleys). They are local extrema, with the abolute minimum of energy lying at the Γ point in the BZ.
[25] The position of the saddle points does not depend explicitly upon the hoppings t_i, and their position is constant only if the lattice remains undeformed.
[26] G. Montambaux, F. Piéchon, J.-N. Fuchs, and M. O. Goerbig, arXiv:0904.2117 (2009).
[27] P. Dietl, F. Piéchon, and G. Montambaux, Phys. Rev. Lett. **100**, 236405 (2008).
[28] This is another way to see why strain along A can never lead to a gap.
[29] This is, of course, the same shift that one obtains using a perturbative Hamiltonian in the hoppings from the outset, in which case one generates the widely discussed effective gauge fields in the low energy description[40].
[30] K. Kishigi, H. Hanada, and Y. Hasegawa, J. Phys. Soc.

Jpn. **77**, 074707 (2008).
[31] M. O. Goerbig, J.-N. Fuchs, G. Montambaux, and F. Piéchon, Phys. Rev. B **78**, 045415 (2008).
[32] K. S. Kim, Y. Zhao, H. Jang, S. Y. Lee, J. M. Kim, K. S. Kim, J.-H. Ahn, P. Kim, J.-Y. Choi, and B. H. Hong, Nature **457**, 706 (2009).
[33] G. Gui, J. Li, and J. Zhong, Phys. Rev. B **78**, 075435 (2008).
[34] Z. Ni, T. Yu, Y. H. Lu, Y. Y. Wang, Y. P. Feng, and Z. X. Shen, ACS Nano **3**, 483 (2009).
[35] M. Farjam and H. Rafii-Tabar (2009), arXiv:0903.1702.
[36] N. M. R. Peres, J. M. B. Lopes dos Santos, and T. Stauber, Phys. Rev. B **76**, 073412 (2007).
[37] Notice that in Ref. 32 the directions x and y are interchanged with respect to our notation.
[38] Although in this case the most common situation is biaxial strain.
[39] N. Ferralis, R. Maboudian, and C. Carraro, Phys. Rev. Lett. **101**, 156801 (2008).
[40] V. M. Pereira and A. H. Castro Neto, arXiv:0810.4539 (2008).
[41] M. M. Fogler, F. Guinea, and M. I. Katsnelson, Phys. Rev. Lett. **101**, 226804 (2009).